Approximation of hindered zonal settling rates for flocculated inorganic/organic composite suspensions in inertial flow conditions

Alexander P.G. Lockwood [a,b,*], Jacob R.L. Rumney [b], Martyn G. Barnes [a], Jonathan M. Dodds [c], Jeffrey Peakall [d], Timothy N. Hunter [b]

[a] *Sellafield Ltd., Hinton House, Birchwood WA3 6GR, UK*
[b] *School of Chemical and Process Engineering, University of Leeds, Leeds LS2 9JT, UK*
[c] *National Nuclear Laboratory, Workington CA14 3YQ, UK*
[d] *School of Earth and Environment, University of Leeds, Leeds LS2 9JT, UK*

ABSTRACT

Inorganic/organic composite nuclear wastes have poor settling properties which hinder major UK decommissioning operations. Improving the settling properties of these wastes and the accurate prediction of settling rates is therefore key. However, constricted access and limited monitoring capability in radioactive environments limits the use of primary material, necessitating the use of surrogate test materials. Herein, an organic laden nuclear waste test material was characterised by examining the surface chemistry, morphology and settling behaviour. A large molecular weight polyacrylamide polymer was deployed to aggregate the organic laden nuclear waste test material. The polyacrylamide successfully flocculated the test material, increasing the zonal settling rate and decreasing the turbidity by one and two orders of magnitude respectively at optimum polymer dose conditions. Whilst displaying steric stabilisation beyond the performance maxima, reductions in flocculant performance were small with no indication of permanent stabilisation at five times the optimum dose. To mitigate risk, it is critical to understand the dynamics of the settling process. Given the porous, fractal nature of the agglomerates, fractal modified hindered settling models were assessed in order to improve predictions at low solids concentrations. In particular, predictive models using drag coefficients compatible with creeping and inertia flow regimes were utilised in tandem with structural and size data to quantify the impact of neglecting inertia drag as favoured by previous literature. It was found that at low solids concentrations, the interparticulate spacing was significant and that inertial flow conditions were integral considerations to achieve close first-order approximations of zonal settling rate.

1. Introduction

The UK is undertaking a massive decommissioning effort to safely dismantle and contain legacy nuclear liabilities. Because the UK was at the forefront of innovation in nuclear industry, in terms of the deterrent, and civil energy production in the 1950s, nuclear waste manifests in a range of different forms depending on the engineering design, material selection and storage strategy of the items [1]. Due to the momentum of technology development, decommissioning was often not part of the lifecycle plan in these endeavours. A particular challenge is spent nuclear fuel from the UK's Pile fuel reactors. The fuel has been held in outside storage facilities open to the weather and foreign contaminants since the 1950s. As the range of fuel stored as part of the Pile fuel

programme is galvanically stable relative to other fuel rod designs, the ponds did not require corrosion mitigation in the form of caustic dosing [2]. This neutral pH at the time the spent Pile fuel was first stored has increased to approximately pH 9 over time, as the pond is not caustically dosed, resulting in an accumulation of biological and organic contamination. Pile fuel storage pond contaminants are known to include algal blooms, bird guano, and foreign object incursion due to the open-air nature of the pond including animal remains as well as sands and silts [3,4]. The composite inorganic/organic nature of sludge that has formed in the Pile fuel storage pond has challenging rheological properties and poor settleability due to the organic fraction of the sludge lowering the material absolute density. This phenomenon is the result of the presence of microorganisms that provide biophysical cohesion, binding silt and

sand, and the absence of such cohesion in morphodynamic models has led to poor prediction [5,6].

Poor water visibility, sub-optimum material transfer and sludge dewatering hinder waste separations and decommissioning operations [3]. Parallel efforts have been made for improving the settling characteristics of a number of nuclear waste sludge types, where one of the strategies that has been suggested is the deployment of high molecular weight polymeric flocculants, to agglomerate colloidal particles and improve dewatering ratios. Similar methods have been shown to be successful in various nuclear and non-nuclear applications [7–10]. A further complexity of the challenge is that leaching of nuclear fission products and minor actinides from the metal fuel bars has complicated pond water chemistry, resulting in a variable electrolyte background, including the presence of polyvalent species that can impact the efficacy of flocculation [2,11–13]. Polymeric flocculants with ionic functionalities are sensitive to electrolyte concentrations, where polyvalent ions can condense around the ionic functional groups, as Debye screening shields like-like repulsion between the polymer segments. Screening causes them to collapse into coil configurations reducing their effectiveness as flocculants [12,14,15]. For organic laden sludge wastes, particularly those contaminated with microalgae, cationic polymers are often deployed to target the phosphate, sulphate and carboxyl surface functionalities to flocculate material [16,17]. However, these cationic flocculants have been poor flocculants for microalgae species found in saline and brackish conditions [18,19].

As a potential solution, non-ionic polymers such as polyacrylamide have more model relaxation and conformation behaviour [20]. They have been found to have resistance to efficacy reduction in the presence of increased electrolyte concentrations at pH ranges similar to the Pile fuel storage pond, as the polymers already possess a coiled configuration in saline conditions [2,15]. As a consequence, non-ionic polymers have been suggested for enhanced oil recovery operations, due to this relative compatibility with saline environments [15]. These non-ionic polymers have also been deployed in wastewater treatment to flocculate biological sludge wastes as well as nuclear wastes [21], whilst investigations have shown their compatibility over a range of inorganic sludges such as clays [22–24]. This resistance to further coil collapse and adsorption affinity for both dipole and ionic surface speciation may be particularly beneficial for the complex challenge of Pile fuel sludge management, making them a potentially flexible treatment aid.

The viability of a nuclear waste treatment solution transcends the optimisation of the technology where safety is an intrinsic factor in determining effective dewatering operations. Nuclear waste management operations require extensive shielding to ensure that workers are not exposed to damaging radiation, and these radioactive environments create challenges to process monitoring technologies. Whilst there are technologies in development to monitor sludge properties in situ [25,26], predicting the settling of sludges is a key capability to optimise clarification residence times in nuclear dewatering activities and related industrial fields [27,28]. The nature of the particulate material in these ponds is known to be weakly aggregated, meaning that agglomerates are porous and fractal in nature [8,29]. This porous structure leads to complexities in hindered settling models such as those proposed by Richardson and Zaki [30], where mathematical adjustment is required to account for the fractal nature of the particles. Currently there is confidence in deploying such correlations to controlled model particles systems (i.e. monodisperse primary particles) but such techniques are becoming more common in real industrial settlings, allowing first order approximation of complex process feed settling behaviour [8,25,31,32]. Furthermore, there is an assumption that concentrated suspensions intrinsically have low settling velocities and very low related particle Reynolds numbers (*Re*) that can be considered to be in the creeping flow regime [33]. Work has been done to apply inertial flow settling considerations to individual fractal floc systems [34–40]. Nevertheless, it is also assumed hindered settling interactions have greater detriment to zonal settling rate in complex flocculated systems, so drag variation is typically considered to be negligible [32].

Previous work by the current authors [41] incorporated inertia drag considerations into fractal modified hindered settling models to improve predictions at low solids concentrations [8]. A similar model augmentation has also been suggested recently in predicting the settling performance of wastewater treatment sludges at varying solids concentrations by Asensi and Alemany [42]. However, as transfers from spent nuclear fuel ponds can vary in concentration [3], it is required to understand if there are conditions where the interparticle spacing of flocs during sedimentation is significant enough that the system could firstly be operating in the inertia flow regime. If inertia drag is significant enough it should be considered in predictive models as it has been shown to be important regarding other nuclear waste test materials [43]. Additionally, previous work [8] has indicated that in polydisperse systems, axial particle-particle interactions are not equal, where larger flocs dominate the settling behaviour and 90th cumulative percentile floc sizes produced the most consistent approximation of zonal settling rates.

In order to understand the structure-property relationships of complex sedimenting flocs more completely, this work investigated an organic laden nuclear waste test material that was prepared in concentrations bordering on the hindered/free settling boundary. The naturally occurring aggregates were firstly characterised to determine the particulate morphology and surface chemistry, whereupon a non-ionic polyacrylamide-based polymer was used to flocculate the test material and the polymer adsorption affinity examined. The floc size and structure were probed using low volume ex situ techniques, including automated single-element microscopy and static light scattering, for size distributions and fractal dimension determination respectively as a function of polymer dose. The settling rate and supernatant turbidity were then determined to identify the steric stabilisation and optimum flocculation performance of the system. Critically, structural and size data could then be used to compare enhanced fractal modified settling models, assuming creeping flow and inertia flow conditions. Here, a sensitivity analysis was performed to understand how the relative influence of size and fractal dimension varies, in order to reduce sources of error in performance prediction to provide improved absolute first-order approximations of zonal settling rate for industrial application.

2. Materials and methodology

2.1. Materials

Experiments were carried out using a storage pond sludge analogue test material sourced by Barrnon Ltd. (Appleby-in-Westmorland, UK) called Appleby sludge. The sludge was derived from a pond situated at an old dairy site in Appleby owned by Barrnon Ltd., which is an open-air environment that has accumulated silt, organic matter and wind-blown debris over the course of a number of years. The sludge was separated by dredging using a drain cleaning vehicle and is known to contain a range of putrefied organics. The material has previously been selected as a radwaste test material by Sellafield Ltd., where it has been proposed that the Appleby sludge surface chemistry is likely representative of pile fuel storage pond sludge. The sludge was held at the National Nuclear Laboratory (Workington, UK) and externally characterised by the SOCOTEC (Burton-on-Trent, UK). Sampling included heavy metal analysis, pH, phenols, volatile and semi-volatile organic compounds, bacterial content, and polycyclic aromatic hydrocarbons; see details in the electronic supplementary material (ESM). The pH was found to be slightly alkali but near neutral which is typical for such farming waste materials [44]. It should be noted that experimental assays regarding concentration range were limited to a single concentration, due to a balance between volume of material and test repeatability. Furthermore, ex situ analysis was limited due to the detection of trace asbestos in the sludge that limited the sampled concentration range.

FLOPAM FA 920 SEP, manufactured by SNF Ltd. (Wakefield, UK)

was selected as a flocculation agent driven by the reagent's compatibility with stringent environmental and nuclear regulation requirements. FLOPAM FA 920 SEP, referred to hereon as 'FLOPAM' is a water-soluble polyacrylamide flocculation agent with a molecular weight of 5×10^6 g·mol^{-1}–15×10^6 g·mol^{-1} large enough to provide bridging flocculation [14]. Stock solutions of FLOPAM were prepared in concentrations of 1000 and 10,000 ppm in deionized water at 25 °C and stirred with a magnetic stirrer bar at 250 rpm for a minimum of 3 h based on manufacturer instructions.

2.2. Methodology

2.2.1. Appleby sludge preparation and characterisation

The sludge as received was heterogeneous, consisting of some large (cm scale) debris, and was initially filtered through a 600 μm sieve to remove the debris and slightly reduce the particle size distribution of the sludge to <1 mm, to be within instrument measurement limits and reduce the suspension settleability. The bulk solids concentration of the sieved sludge was then measured by differential evaporation and found to be 5.4 wt%. The initial zonal settling rate of the material was measured using 250 mL measuring cylinders, and the sludge was found to display two phase behaviour, a larger particulate α-phase which settled quickly and a suspended β-phase which was slower settling and diffuse (see Fig. 1). The particle size distribution of the combined phases was characterised using focused beam reflectance measurement (see Section 2.2.3) and the zonal settling rate of the material was also recorded.

Dried sludge samples were characterised using scanning electron microscopy (SEM) (Hitachi SU8230 scanning electron microscope; Hitachi Hightech) to investigate the structure and morphology of the particles and the surface elemental composition was identified using energy dispersive X-ray (EDX) spectroscopy. The sludge was dried and coated in 10 nm of Iridium prior to imaging. The absolute density of the

dried material was identified using a Pycnomatic ATC Helium Pycnometer (Thermo-Fisher Scientific, UK) and determined to be 1417 kg·m^{-3}. To achieve conditions that are more industrially analogous to nuclear pile fuel storage ponds the initial sludge suspension was diluted, reducing the solids concentration to 1.19 wt% (0.84 vol%). A sample of the β-phase of the diluted sludge was taken and the zeta-potential was identified via electrophoresis using a Zetasizer Advance (Malvern Panalytical, UK).

2.2.2. Flocculation procedure

Firstly, 250 mL of the dilute sludge was transferred to a 4 L baffled tank used in previous work [8] equipped with an overhead stirrer and a 48.2 mm 60° pitch blade impeller with a 1 cm clearance from the base of the reactor vessel and was mixed at a rate of 200 rpm to ensure that particulates were fully suspended. Flocculant was transferred via micropipette from the 1000 and 10,000 ppm stock solutions to achieve concentration ranges of 1.25–100 ppm of FLOPAM in the bulk solution. The mixture was then left to flocculate for 5 min before being transferred to a 250 mL measuring cylinder for multiple analysis purposes. Whilst shear is an important factor in flocculation efficacy, which deserves an isolated investigation, rotation rate selected in this work based on this previous investigation [8] to standardise material preparation, and isolate the effects of concentration of FLOPAM on settling and overdose behaviour.

2.2.3. Focused beam reflectance measurement (FBRM)

Focused beam reflectance measurements using model PI-14/206 (Mettler-Toledo, USA) were conducted in situ to identify the chord length distribution of the combined α and β phases of the suspended sludge, as well as the supernatant β-phase post sedimentation. Here, 2 L of the unfiltered sludge (minus larger refuse debris) was transferred into the baffled reactor vessel and mixed, as per the flocculation. The FBRM probe was inserted into the suspension at a 60° angle (to prevent
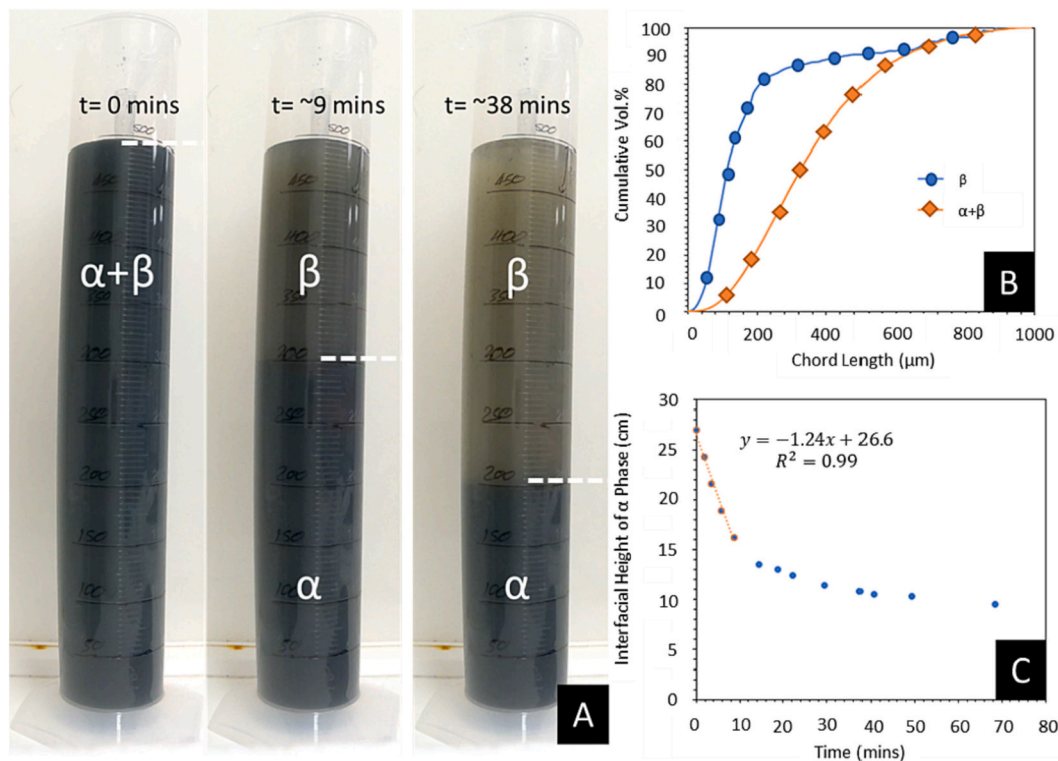
Fig. 1. A) Settling images of 5.4 wt% Appleby sludge at 0, 9 and 38 min, where the α-phase refers to the larger particulate fraction of the material which displays strong settling characteristics and β-phase refers to the finer fraction of the sludge particle sizes which results in a diffuse turbid supernatant. B) The cumulative frequency distribution obtained by a focused beam reflectance meter (FBRM) displaying the combined α and β and the separated β-phase chord length distributions. C) Zonal interface height with time, with the averaged gradient of the initial linear region shown.

particulates sticking to the probe lens and providing sufficient flow across the lens without generating dead zones) with a 2 cm clearance from the reactor vessel base. The FBRM was operated in macro-mode with a scanning velocity of 8 m·s^{-1} and a measuring frequency of 15 s^{-1} for 1 h. Data were computed on a volume basis and translated to a cumulative frequency distribution.

2.2.4. Automated single element microscopy

Visual microscopy was also utilised to confirm the size and morphology of aggregates produced from suspensions dosed with 1.25–10 ppm polymer concentration, using a Morphologi G3 (Malvern Panalytical Ltd.) automated single element microscope. Floc samples were prepared in the same manner as described in Section 2.2.2, whereupon 5 mL aliquots were sampled using a wide bore micro-pipette and placed onto four microscope slides and analysed optically with three repeats. Data were analysed both in terms of circular equivalent diameters and aspect ratio.

2.2.5. Static light scattering

Static light scattering (SLS) was used to measure both the fractal dimensions of flocculated suspensions. The SLS measurement process can impart shear on the flocculated material resulting in floc breakdown and densification, so measurements were repeated in triplicate with fresh flocculated samples as highlighted in the authors' previous work [8]. Here, 250 mL suspensions were flocculated with 1.25–10 ppm of FLOPAM for 5 min, as described in Section 2.2.2. The suspensions were then transferred to a 250 mL measuring cylinder and inverted 5 times to meet the shear conditions in the sedimentation tests (Section 2.2.6). A 5 mL aliquot was then drawn from the measuring cylinder and added to a Mastersizer 3000 (Malvern Panalytical Ltd) using a Hydro 3000 Mv aqueous dispersion cell (external dimensions of 180 mm × 280 mm × 300 mm and sample volumes between 50 and 120 mL). The Hydro MV dispersion unit was prefilled with 120 mL of deionized water. Importantly, the unit was sheared at 900 rpm to ensure consistent flow of suspensions through the vertical optical window and to prevent particle deposition, meaning that there was some potential for additional shear degradation of the generated flocs. Floc size distribution data were generated from the Mastersizer 3000 as Mie theory based SLS, using a 4 mW He-Ne, 632.8 nm laser via Eq. (1). For each experiment, the scattering intensity is a function of the magnitude of the scattering wave vector, Q, a reciprocal of the particle size, where n is the refractive index, λ is the wavelength of the incident light in vacuo and θ is the scatter angle shown in Eq. (1). It should be noted as the material is heterogeneous and multiphase, a refractive index was assumed to be representative of aluminosilicates due to the EDX analysis of the sludge see (ESM Fig. S1) where $n = \sim 1.5$.

$$Q = \frac{4\pi n}{\lambda} \sin(\theta) \tag{1}$$

The fractal structure of the sludge particles is determined using relationships developed by Mandelbrot [45], and the procedure of relating the linear function of the scatter wave vector, Q, and the scatter intensity, $I(Q)$, is thoroughly discussed in a comprehensive review by Sorensen [46]. The proportionality below shows that $I(Q)$ is proportional to the Q to the power of the fractal dimension. By plotting Log[$I(Q)$] and Log[Q], the negative fractal dimension can be obtained from the linear segment of the plot [46,47].

$$I(Q) \propto Q^{-d_f} \tag{2}$$

For a fractal structure, the density decreases as you move from the centre to the edges. This allows a calculation of an effective hydrated density of the flocs of symmetrical structure i.e. $\nabla \rho = f(r_i, d_f)$ where r_i is distance between the geometric centre of the structure to its radii. The relationship between the number of primary particles in a minimum repeating floc unit, N, and the floc properties; including the diameters of the minimum repeating floc unit and primary particles, D_f and D_p

respectively, and the fractal dimension d_f are shown in Eq. (3).

$$N = \psi \left(\frac{D_f}{D_p} \right)^{-d_f} \tag{3}$$

The values of D_f and D_p are determined by the corresponding inverse logarithmic reciprocal scatter wave vectors at the bounding limits of the linear part of the Log[$I(Q)$] and Log[Q] plots as described by Sorensen [46] and Lockwood et al. [8]. The structure prefactor, ψ, is related to the fractal dimension of the material and has been linearly correlated between $1.5 \leq d_f \leq 2.75$ by Gmachowski [48] in Eq. (4).

$$\psi = 0.414 d_f - 0.211 \tag{4}$$

It is then possible to use the number of primary particles in a floc to calculate the floc density if sphericity is assumed, as discussed by Bushell et al. [34] and shown in Eq. (5). Here, the subscripts p, f and w refer to particles, flocs and water respectively and V and ρ are volume and density respectively. As a result, ρ_f is the effective hydrated floc density.

$$\rho_f = \frac{(NV_p\rho_p) + (V_f - NV_p)\rho_w}{V_f} \tag{5}$$

2.2.6. Zonal settling rate and supernatant quality

The zonal settling rate of the suspensions was determined by first flocculating and mixing the sludge, as outlined in Section 2.2.2, before transfer to 250 mL measuring cylinders, where the zonal settling rate was tracked. The linear section of the settling curve was then fitted, and the zonal settling rate determined from the gradient. The supernatant quality was assessed by taking aliquots of the supernatant after 10 min from a depth of 5 cm from the air water interface. The turbidity of the β-phase supernatant was obtained using a TN-100 turbidity meter (Eutech Instruments) reported in Nephelometric Turbidity units (NTUs) as is common in literature for post-polymeric settling supernatant quality [15,49]. The total organic carbon content determined using a Jena Multi N/C 2100 (Analytik Jena, Germany) analyser to measure total organic carbon (TOC) differentially. The material was flocculated as per Section 2.2.2 and transferred to a 250 mL settling cylinder for concentrations between 0 and 10 ppm for FLOPAM. The material was then allowed to settle completely and an aliquot from the supernatant was taken. Furthermore, background samples of FLOPAM were prepared in Milli-Q® water (0–10 ppm). Additionally, FLOPAM controls were analysed as dosed concentrations, to determine the expected carbon concentration if no adsorption were to take place, to assess the degree of flocculant adsorption onto the sludge.

2.3. Sedimentation modelling theory

The fundamental model to estimate the zonal settling rate of suspensions considered here, was first proposed by Richardson and Zaki [30] shown in Eqs. (6) and (7). Here, f_s is the functional permeability, U_T is the terminal velocity of the aggregate floc and U_z is the zonal settling velocity of the suspension interface. In the Stokes terminal velocity model in Eq. (7), the size term, $\overline{D_f}$, is a single number to represent the diameter distribution of the flocs in suspension, which in this work will refer to the volume weighted average ($d_{4,3}$) or the 90th cumulative percentile size of the flocs (d_{90}). In terms of the functional permeability, f_s, part of Eq. (7), Φ represents the particle volume fraction and R_z is the Richardson-Zaki exponent, a non-linear modifier capturing effects of water displacement in suspension dewatering that is often a function of Reynolds number in literature [66]. For spherical particles at low Reynolds number, it is assumed to be ~4.65, and this value is used here.

$$U_Z = U_T \times f_s \tag{6}$$

$$U_z = \frac{(\rho_p - \rho_w)\overline{D_f^2}g}{18\,\mu_w} \times (1 - \Phi)^{R_z} \tag{7}$$

The model applies a functional permeability term to the Stokes terminal settling velocity to account for steric and flow regime changes by fluid displacement of settling particles resulting in hindered settling. Adaption of the Richardson-Zaki model has been attempted to account for variables such as sphericity and fractal density and has been used previously in work directly applicable to the nuclear industry [8]. Eq. (8) shows a fractal modified settling model as utilised and by Vahedi and Gorczyca [39], Qasim et al. [50] and Winterwerp [51] to predict the individual terminal velocity of flocculated clays and kaolinite respectively. It incorporates the drag correlation of Schiller and Naumann [52] through the floc Reynolds number (Eq. (9)) to account for any enhancement to fluid drag at high settling velocities. Whilst there is a number of intermediate regime ($0.3 < Re < 500$) drag correlations within the literature, changes between these fits are significantly less impactful than comparing to the creeping flow regime [33]. Therefore, a single well-established inertial flow drag coefficient was selected for this work [34–40,52].

$$U_T = \frac{(\rho_p - \rho_w)g}{18\mu_w} D_p^{3-d_f} \frac{\overline{D_f}^{d_f-1}}{1 + 0.15Re^{0.687}} \tag{8}$$

$$Re = \frac{U_T \rho_W D_f}{\mu_w} \tag{9}$$

To account for the increase in effective volume fraction of the flocs (rather than only considering the volume fraction of the discrete particles), the functional permeability term, f_s, is modified to include the fractal properties, as shown in Eq. (10).

$$f_s = \left(1 - \Phi \left(\frac{D_f}{D_p}\right)^{3-d_f}\right)^{R_Z} \tag{10}$$

For many flocculated systems (of relatively large D_f/D_p) this often results in the functional permeability term dominating behaviour and therefore the suspension conditions can be assumed to be in creeping flow conditions [32]. However, previous work by Lockwood et al. [8] suggests that floc-floc interactions are present, manifesting primarily as sweeping flocculation where larger flocs encompass smaller flocs and dominate the settling behaviour. It was also suggested that the ratio of inter-particle and intra-particle spacing are important considerations when predicting zonal settling rates of flocculated suspensions. For dilute suspensions, the inter-particle spacing is much larger than intra-particle spacing, meaning fluid flow around flocs is likely more favourable than through their fractal structures as suggested by Xiao, Lam, and Li [53], meaning that the effects of functional permeability are diminished, and improved settling velocities could cause a creeping flow-inertial flow transition.

Given the aforementioned points, it is suggested that the overall Fractal Modified Richardson-Zaki (FMRZ) hindered settling model (Eq. (11)), as utilised by Heath et al. [32], Lockwood et al. [8] and Hunter et al. [25] should incorporate drag coefficients representative of inertial flow conditions. Lockwood et al. [41] suggested that the inertial flow representative fractal settling model utilised by Vahedi and Gorczyca [39] can be combined with the fractal modified functional permeability term in the FMRZ model to produce an inertial modified FMRZ model referred to hereon as the '*i*-FMRZ' model; see Eq. (12). This model is similar to the recent proposal of Asensi and Alemany [42].

$$U_Z = \frac{(\rho_p - \rho_w)\overline{D_f^2}g}{18\mu_w} \left(\frac{D_f}{D_p}\right)^{d_f-3} \left(1 - \Phi \left(\frac{D_f}{D_p}\right)^{3-d_f}\right)^{R_Z} \tag{11}$$

$$U_Z = \frac{(\rho_p - \rho_w)g}{18\mu_w} D_p^{3-d_f} \frac{\overline{D_f}^{d_f-1}}{1 + 0.15Re^{0.687}} \left(1 - \Phi \left(\frac{D_f}{D_p}\right)^{3-d_f}\right)^{R_Z} \tag{12}$$

3. Results and discussion

3.1. Physical characterisation and separation of the flocs

3.1.1. Appleby sludge baseline behaviour

A baseline understanding of the sludge behaviour and properties was required before deployment of the flocculant to aggregate the material. Fig. 1A shows the settling behaviour of the non-diluted sludge, with clarification into lower consolidated α-phase and a supernatant liquor (β-phase) after 38 min. It should be noted that below the zonal interface is a mix of α and β phase and not α-phase alone. The chord lengths of the combined αβ-phase and slow settling β-phase were probed using a focused beam reflectance measurement (FBRM) as shown in Fig. 1B. The αβ-phase exhibits particulates with larger chord lengths than the β-phase, unsurprisingly. The zonal settling rate obtained from tracking the interface of the αβ-phase is given in Fig. 1C, with the initial zonal settling rate being found to be 1.24 cm·min^{-1}. Whilst the entire suspension is heterogeneous, the β-phase is the material that a polymeric flocculant must target to reduce supernatant turbidity, as the α-phase has adequate settling characteristics.

Particle morphology of the sludge was probed using scanning electron microscopy, as presented in Fig. 2A–D(ii). In all figures, the bulk particulates appear to be made of agglomerates of much smaller primary
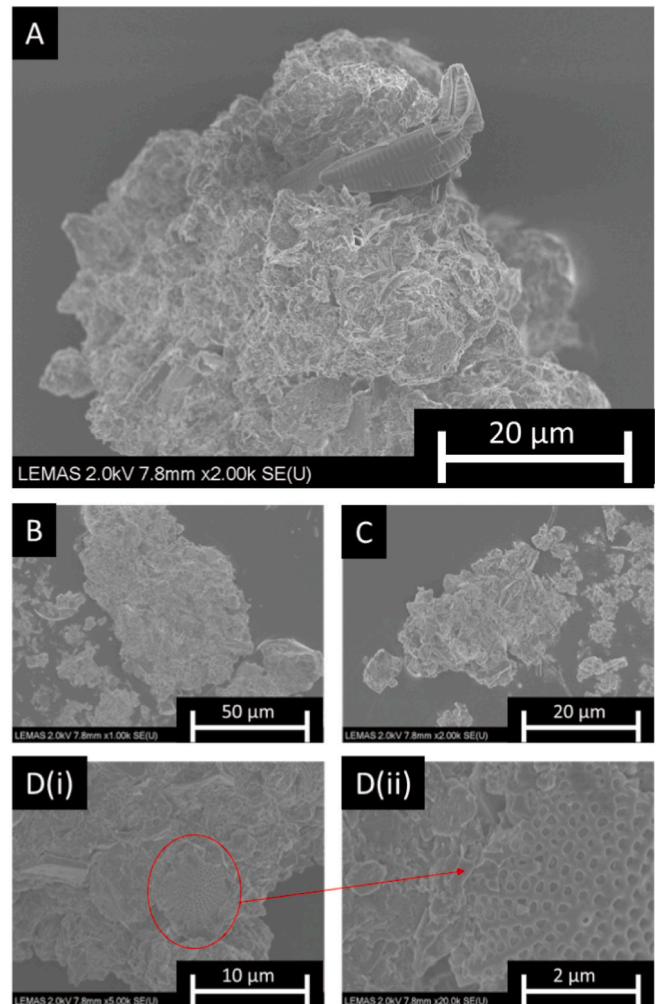
Fig. 2. Scanning electron micrographs of Appleby sludge. A, B and C show images of different particles at 20, 50 and 20 μm scales respectively. D(i) and D (ii) are the same particle imaged at 10 and 2 μm scales to highlight the presence of a diatom. The red circle on D(i) depicts the area D(ii) is zoomed from, focusing on a diatom structure.

particles, however, with quite compact structures. It appears similar to granular anaerobic sludge particles obtained from the brewery industry by Caizán-Juanarena et al. [54]. Additionally, as the dried sludge material displayed an absolute dry density of ~1440 kg·m^{-3}, it indicates there may be a large organic component to the wastes (as most inorganic silts and clays have densities >2500 kg·m^{-3}). Mixed anaerobic sludges harvested from the municipal wastewater treatment plant in Utrecht have been reported to have densities of 1027 kg·m^{-3} when examined with pycnometers [55] and research into fractal properties and hindered settling models in wastewater treatment sludges by Asensi and Alemany [42] found very similar absolute solid densities of 1710 kg·m^{-3}. Fig. 2A and D(i) and D(ii) show the presence of diatoms (single cell algae) including pennate and centric morphologies in Fig. 2A and D respectively [5]. Micro-organisms such as diatoms secrete cohesive extracellular polymeric substances (EPS) [5], and their presence suggests that the sludge consists of clay and silt structures bioflocculated by EPS into low density organically dominated structures. The surface elemental composition was probed using energy dispersive X-ray (EDX) spectroscopy (see the ESM), showing varying elemental composition across the surface of sludge particles with some surface species indicating the presence of carbonate and oxide species with low Si concentrations along with evidence of organic structures.

3.1.2. Polymer adsorption and floc structure

The surface potential of the sludge particles without polymer is displayed in Fig. 3A. The distribution has a small span (~−5 to −25 mV), with an average zeta-potential of −13.46 mV. It should be noted that this is the fine segment of the particle size distribution and does not represent the entirety of the suspension, although, this suspended, fine size fraction (the β-phase) is the most problematic for settling residence times and is a priority for the FLOPAM to target and flocculate. This anionic zeta-potential is consistent with the constituent elements of the sludge, where clays such as kaolinite and montmorillonite display zeta potentials at neutral pH of >−30 mV [49,56] due to the presence of deprotonated silanol (-Si-OH) and aluminol (-Al-OH) surface groups. Additionally, aggregation of microalgae is generally prevented by electrostatic repulsion caused by the negative surface charge of the cells due to the presence of carboxyl, sulphate or phosphate groups on microalgae cell surfaces [16]. The affinity of the FLOPAM to the sludge particle surface was tested using the differential supernatant total organic carbon concentration procedure. Presented in Fig. 3B is the determined carbon concentration from TOC measurements from both the polymer only, in increasing concentrations, as well as that taken from the supernatant of settled suspensions with the same flocculant addition. It is clear from the baseline that as the concentration of FLO-PAM increases, the carbon concentration increases proportionally, as

expected. Interestingly by contrast, the supernatant concentration remains reasonably consistent against the reading without any flocculant addition. This independence indicates that the addition of FLOPAM is having little observable effect on the carbon concentration in the supernatant, suggesting a high adsorption affinity for the sludge surfaces. Whilst this is not explicitly demonstrated, it is unlikely any organic transfers are occurring to balance the concentration of carbon with increasing flocculant concentration.

Based on the anionic surface potential characteristics shown in Fig. 3A, the high affinity of the FLOPAM is surprising, as the FLOPAM is non-ionic and has a lower electrostatic potential between the polymer functional groups and sludge surface species and for this reason cationic polymers are generally selected to dewater microalgal laden wastes in literature [16]. The polymers in literature tend to have a cationic quaternary ammonium functionality (such as poly(dimethylaminoethyl methacrylate)) which have an affinity for anionic surfaces [17]. It is good practice when facilitating bridging flocculation to use high molecular weight statistical copolymers of an ionic functionalised monomer in conjunction with acrylamide backbone, as flat conforming polymer chains lack the ability to extend beyond the Debye layer of particles to facilitate flocculation, though in some cases localised charge reversal from dense adsorption of polymer can facilitate charge patch flocculation [14]. A study by Nasser and James [49] investigated the flocculation of kaolinite using cationic (quaternary ammonium functionality) and anionic polymers (carboxyl functionality). The anionic polymers had much lower adsorption density when compared to the cationic polymers but flocculated the kaolinite to larger sizes with faster settling rates. Nasser and James [49] postulated that the dipole on the amine functional group of the polyacrylamide facilitated hydrogen bonding of the polymer onto the kaolinite silanol and aluminol surface groups.

So, when considering the relative affinity of the non-ionic polymer in this work to the cationic polymers deployed in literature [16], the presence of microalgae alone is unlikely to be contributing to the strong adsorption affinity, as non-ionic polymers have been found to be inefficient at flocculating microalgae in marine and freshwater conditions [18,57]. Another mechanism, when considering algal laden sludge material, is that pennate and centric diatom single cell algae secrete EPS which may provide sites that the FLOPAM can form strong van der Waals and/or hydrophobic interactions with [14]. When combined with potential dipole-ionic and hydrogen bonding adsorption mechanisms on inorganic sites, this may provide the comparatively high adsorption affinity suggested by Fig. 3B. In terms of nuclear waste disposal, whilst the high degree of adsorption reduces any potential threats to downstream processes, it also means that there will be a high burden of polyacrylamide in the selected final waste form for solids disposal.
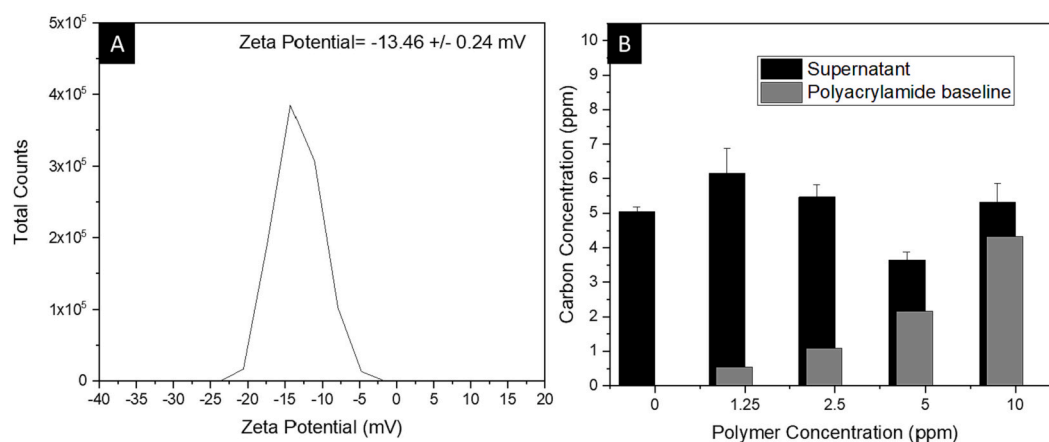
Fig. 3. A) the zeta-potential distribution of Appleby sludge material without flocculant taken from the β-phase of the suspension. B) Total organic carbon concentrations of FLOPAM flocculant, as a function of polymer baseline concentration, as well as from the supernatants of flocculated suspensions.

Depending on the disposal method, compatibility with grouting processes would need to be understood, although if thermal treatment is selected, the risks to the geological disposal facility, in terms of radionuclide chelating degradation products from radiolysis and alkali hydrolysis, would be removed [58].

The structure and fractal nature of the sludge as a function of different concentrations of FLOPAM (0–10 ppm) was interrogated through static light scattering as detailed in Section 2.2.5. The logarithmic scatter intensity, I(Q), as a function of logarithmic scatter wave vector is plotted within the ESM (Fig. S2A) along with the variation of the determined number of particles within the floc, and the resulting floc density versus polymer concentration (Fig. S2B). Corresponding values for calculated minimum repeating floc diameter, D_f, discrete particle diameter, D_p, and fractal dimension, d_f, are displayed in Table 1. The average number of particles, N, in a minimum repeating floc unit and effective floc densities, ρ_f, are also shown in Table 1 (calculated using Eqs. (3) and (5) respectively). Without addition of FLOPAM, the sludge displays a fractal dimension of 2.24 and a calculated effective floc density of 1106 ± 6 kg·m^{-3}. In previous work looking at the fractal dimension of lime softening clays by Vahedi and Gorczyca [59] measured fractal dimensions were found over a range of 2.55 to 2.99 (avg. 2.73) using a box counting technique. As the box counting technique is a single-element analysis, the trend between floc size and fractal dimension was found to be inversely related, whereas as flocs grow, their fractal dimension decreased. However, when investigating the fractal dimension indirectly using settling, the fractal dimension was found to be 1.87. The discrepancy between the two measurements has also previously been highlighted by Glover et al. [31] who studied the fractal dimension of flocculated alumina using a static light scattering technique (giving a fractal dimension of 2.12) whereas the indirect settling technique generated fractal dimensions of 1.85. There is some uncertainty regarding the effectiveness of SLS with polydisperse primary particle systems, but incorporation of this mathematical fidelity into practical settling models has not yet been established [31,59]. The lime softening clay flocs analysed by Vahedi and Gorczyca [59] have greater fractal dimensions than the sludge in this work when considering direct measurement, which is likely due to the aggregative nature of the clays and lack of organic flocculation facilitated by the EPS in this work. Similar research into fractal properties in wastewater treatment sludges by Asensi and Alemany [42] found that activated sludges had a fractal dimension range of 2.27–2.39, which is in line with the data here. It should also be mentioned that preparation conditions can affect the fractal dimension of flocs as they are particularly sensitive to shear and are known to densify overtime [8,60].

Upon addition of FLOPAM, there are slight increases in the fractal dimension (Table 1) from 2.24 to 2.29 over a concentration range of 0 to 10 ppm. Similar increase in fractal dimension with polymer dose was observed by Jarvis et al. [61] who flocculated wastewater containing anionic surface potential natural organic matter also using non-ionic polymer. Also shown in Table 1 is the minimum repeating floc size which increases with polymer dose. Whilst the solids phase of the flocs increases slightly with fractal dimension, the increase in floc size overall results in a decrease in effective floc density, as N increases. This decrease in floc density with increasing incorporation of primary

Table 1
The calculated fractal values of fractal dimension, d_f, the average number of particles in a minimum repeating floc unit, N, the diameter of minimum repeating floc unit, D_f, the diameter of the primary particles in a floc, D_p, and the effective hydrated floc density, ρ_f.

Polymer conc. (ppm)	d_f	N	D_f (µm)	D_p (µm)	ρ_f (kg·m^{-3})
0	2.24	18 ± 3	6.3 ± 0.4	1.6	1106 ± 6
1.25	2.25	28	6.7	1.3	1090
2.5	2.29	41 ± 12	8.4 ± 0.5	1.5 ± 0.1	1091 ± 9
5	2.30	62 ± 17	10.0 ± 0.6	1.5 ± 0.1	1082 ± 9
10	2.29	83 ± 10	14.2 ± 0.8	1.8 ± 0.1	1071 ± 4

particles is typical of fractal floc systems [62,63].

The cumulative frequency size of the flocs produced from dosing regimens of 0–10 ppm of FLOPAM are shown in Fig. 4A, with the volume weighted average ($d_{4,3}$) and the 90th percentile cumulative volume floc size (d_{90}) values shown in Fig. 4B. Some example images of flocs produced at the 5 ppm dose are shown in Fig. 4C(i) and C(ii) at 200 µm and 20 µm scale respectively, suggesting open porous structures similar to other flocculated radwaste test materials in literature [8]. Fig. 4A and B clearly indicates that as flocculant dose is increased over the range of 0–10 ppm, there is a significant increase in corresponding floc sizes, although, whilst there is a rapid increase between 0 and 5 ppm, the size begins to plateau between 5 and 10 ppm. It is likely the flocs are approaching a maximum adsorption density. At this point, the effectiveness of the bridging flocculation mechanism between the sludge particles begins to wane as less active adsorption sites are available, or there is a steric barrier between the layers of unformed coils of polymer on the sludge particle surface [14].

3.1.3. Flocculation effect on zonal settling rate and turbidity

The impact of FLOPAM on settling behaviour was probed over the same 0–10 ppm dose range, as presented from selected images in Fig. 5A after 1 min of settling. The clarity of the supernatant can visually be observed to increase with increasing dose of flocculant, where the height of the zonal settling front also decreases at the 1 minute time with dose. The measured zonal settling velocities for the sludge with flocculant additions over a much larger concentration range (0–100 ppm) is given in Fig. 5B where the corresponding supernatant turbidity after 10 min is shown in Fig. 5C. The optimum initial zonal settling velocity was found to be at ∼20 ppm, where the settling velocity marginally decreases again beyond this concentration up to 100 ppm. The corresponding turbidity readings follow an inverse relationship, with the lowest measured turbidity also being found at 20 ppm, indicating the highest efficiency dewatering concentration in addition to lowest residence time.

Key observations are the zonal settling maxima and turbidity minima in Fig. 5B and C respectively. The performance inflection point typically represents the point of steric stabilisation. Here, the coverage of polymer on the surface of the primary particles prevents polymer tails and loops on the surface of other particles 'bridging' primary particles together by occupying active attachment sites or by unconfirmed coils on both particles sterically [14]. This steric stabilisation phenomenon was observed by Nasser and James [49] in their investigations of flocculation of kaolinite. There are also indications that steric stabilisation may occur in similar organic laden systems analogous to this work, as in the work by Jarvis et al. [61]. It is interesting that in this current work, it is evident that polymer dose up to five times the optimum concentration does not result in permanent or slow settling suspensions, and manifests rather as small reductions in performance more relatable to a plateau than a detrimental change in settling performance. It is likely that the uncharged nature of the polymer may reduce critical overdose issues (as charged polymers will lead to both steric and charge repulsions at high concentrations). Due to the uncertainty around solids contents in nuclear waste streams, this plateauing of settling behaviour with polymer dose reduces the risk in deploying such settling aids, as the sludge in the β-phase is unlikely to be drastically stabilised to the point of colloidal behaviour. Whilst it is possible that the shear conditions in this work also limit the degree of flocculation [8], the displaced fluid from settling flocs could transport sterically stabilised particulates and unflocculated colloidal material through the inter-particle spacing in the suspension which is reflected in the increase in turbidity in Fig. 5C at dosages >10 ppm. However, shear degradation due to excessive mixing would likely produce smaller flocs but be larger than primary particles. Smaller flocs would still be better captured through sweeping flocculation interactions indicated by the use of larger floc sizes to accurately predict performance and would likely not result in an increase in the turbidity observed in Fig. 5C as they would be contained in the αβ-phase.
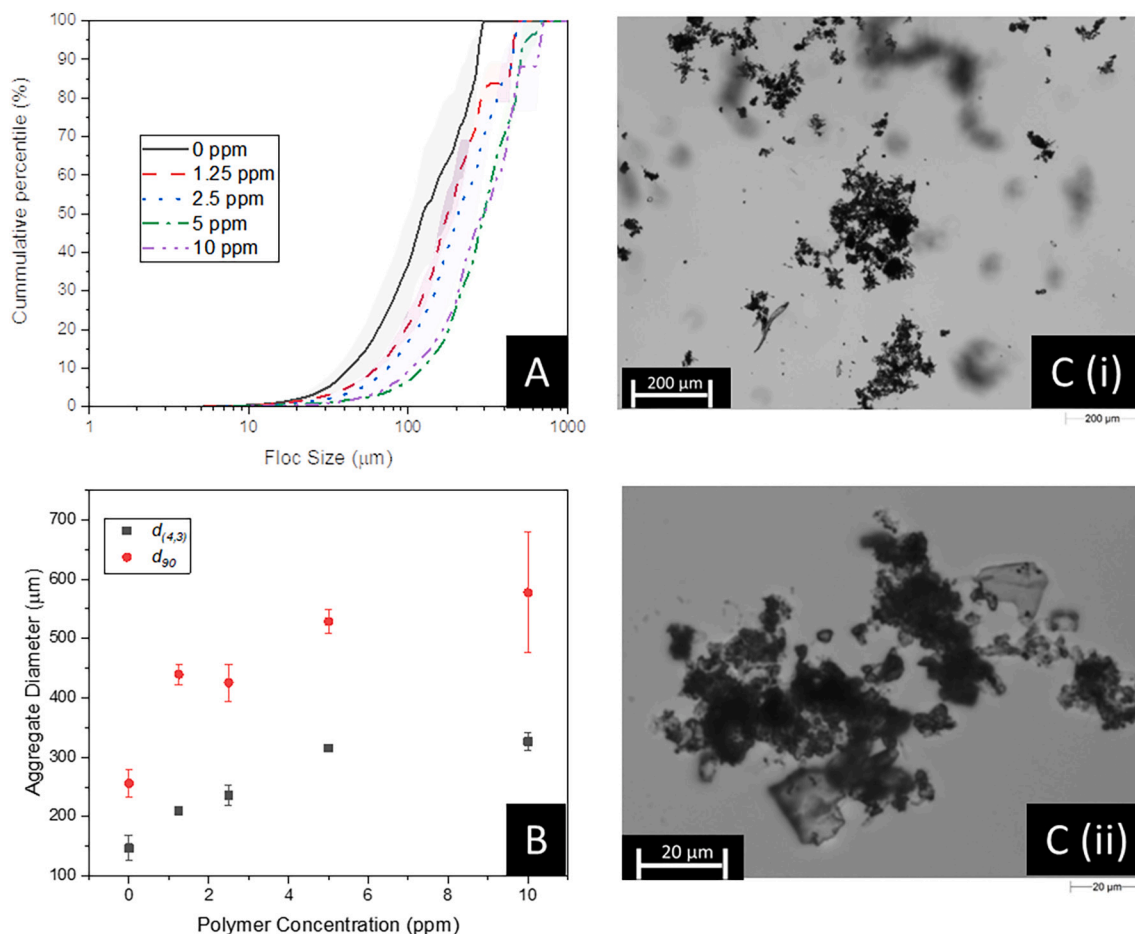
Fig. 4. A) Cumulative frequency particle size distributions (volume weighted) of sludge flocculated with 0–10 ppm FLOPAM by single element microscopy after flocculation for 5 min at 200 rpm. B) Related change in volume weighted floc size ($d_{4,3}$) and 90th cumulative percentile (d_{90}) floc size. C is optical micrographs of a floc dosed at 5 ppm FLOPAM at (i) 200 μm scale and (ii) 20 μm scale.

3.2. Sedimentation modelling and experimental data comparison

3.2.1. Creeping versus inertial flow model multivariate analysis

A multivariate analysis of the FMRZ model, Fig. 6A, and the inertia modified 'i-FMRZ' model, Fig. 6B, was conducted to isolate the impacts of floc diameter, $\overline{D_f}$, and fractal dimension on the zonal settling rate of the flocculated sludge suspensions. Firstly, as fractal dimensions approach 3, the two model outputs appear to converge on each other, especially at larger floc sizes. The differences between the models are present at fractal dimensions <2.5. Below $d_f = 2.5$, the effect of floc diameter is less impactful on zonal settling rate in the i-FMRZ model. This is because the drag coefficient in the FMRZ model is inversely proportional to particle Reynolds number, $U_z \propto 24/Re$, whereas the drag coefficient proposed by Schiller and Naumann [52] in the i-FMRZ model is a non-linear relationship, repressing increases in zonal settling velocity with increasing floc diameter by increasing the drag coefficient with settling velocity. As the fractal dimension approaches 3, $\left(\frac{D_f}{D_p}\right)^{3-d_f}$ in the terminal velocity function, U_t, and $\left(\frac{D_f}{D_p}\right)^{d_f-3}$ in the function permeability, f_s, of the suspension approach unity. Thus, for high fractal dimensions, the effect of Reynolds number function becomes reduced, with respect to aggregate size, which becomes more impactful on the zonal settling rate of the suspensions in both models. However, for systems with lower fractal dimension (more open, porous flocs) the i-FMRZ model is more sensitive to drag, with increasing floc sizes producing relatively lower zonal settling rates in comparison.

Whilst the i-FMRZ model is sensitive to the Richardson-Zaki

exponent, our previous work [41] into projecting the zonal settling rates of Mg(OH)$_2$ based nuclear wastes in the presence of novel diblock polymers has scrutinised the impact of the Richardson-Zaki exponent in detail in a multivariate analysis. The original drag correlation proposed by Schiller and Naumann [52] is valid for $Re > 0.3$. In our work particle Reynolds number is in the order of $Re > 0.3$, when using the d_{90} value, but when using the $d_{4,3}$, the $Re < 0.3$ meaning the i-FMRZ model does not satisfy inertial flow conditions and the FMRZ model should be considered which is much less accurate as per Fig. 6. Particle Reynolds numbers generated in this work used the correlation of Reynolds number and the Richardson-Zaki exponent suggested by Garside and Al-Dibouni [64], where exponent projections from the Garside and Al-Dibuouni correlation compute values of 5 to 4.9. This range has been shown in our previous work [41] to have negligible impact on the zonal settling rate, as values of $n > 5.5$ are expected to introduce substantial hindrance. Therefore, the value for n is taken to be 4.65 for variable isolation and for comparison to previous work [8,32,41].

3.2.2. Comparison to experimental data and sensitivity analysis

Comparing the model performance to experimental data, the FMRZ and i-FMRZ models were used to compute a zonal settling rate, which was plotted on a parity chart against observed zonal settling rates in Fig. 7. As the flocculated and raw particle size distributions are polydisperse, the selection of a single average floc size to represent the whole population is implicitly impactful on the computed zonal settling rate prediction. In the authors previous work [8], into flocculating Mg(OH)$_2$ based nuclear waste simulant sludges using anionic polymers, it was
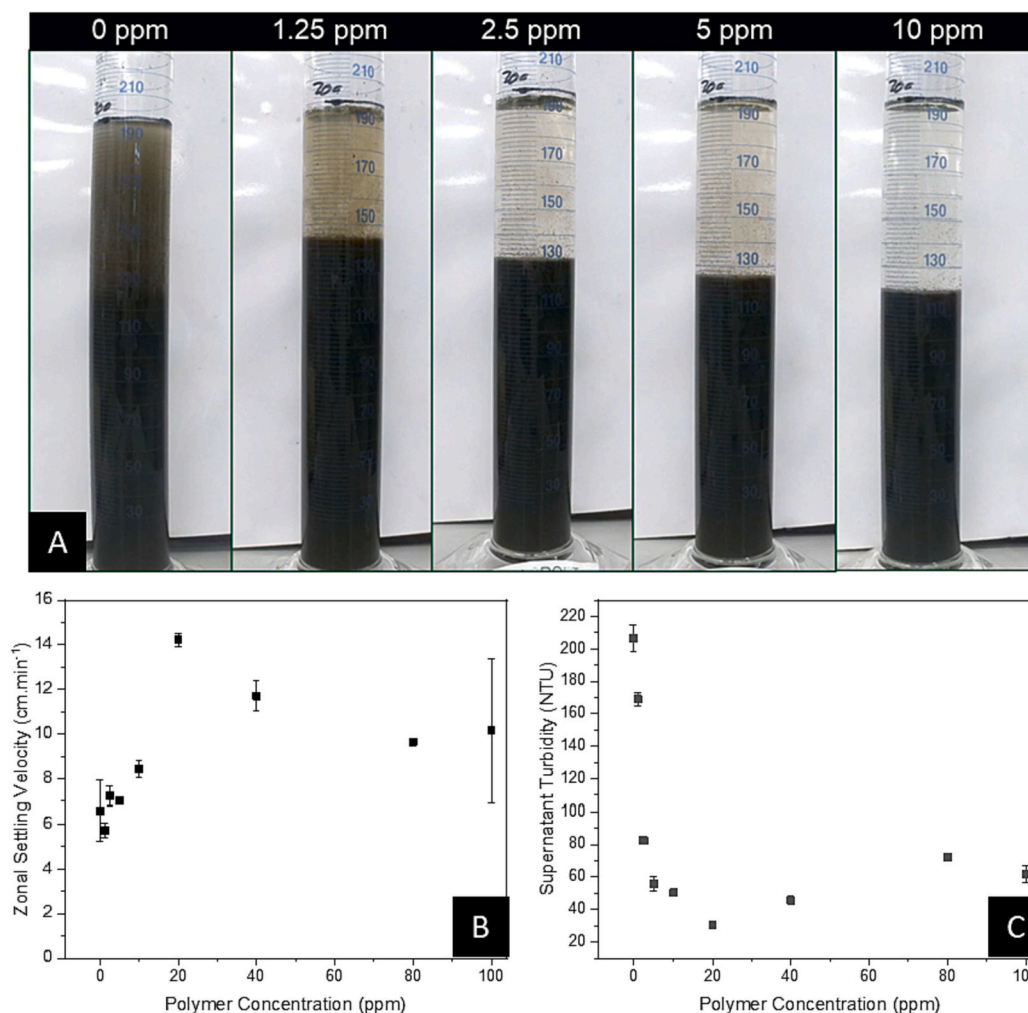
Fig. 5. A) Images of the settling experiments at doses of FLOPAM between 0 and 10 ppm, taken after 1 min of settling. B) The initial zonal settling rates of the flocculation suspensions for a larger 0–100 ppm dose range of flocculant. C) The supernatant turbidity of the suspensions taken from 5 cm below the air-water interface after 8 min of settling.

found that measured d_{90} sizes consistently produced the most accurate predictions, rather than mean sizes. This factor was attributed to the influence of larger flocs encompassing and netting slower settling smaller flocs in their path, and thus dominating the settling characteristics of the suspension. Though there were some disparities between predictions and observations, this was mainly attributed to the internal permeability of the flocs, which is not accounted for in the FMRZ model and has been shown to have an important baring on dewatering in simulations [53].

Interestingly, for the comparisons given Fig. 7A & B, the FMRZ model drastically over predicts the settling rates in all cases, with mean absolute percentage errors (M.A.P.E., provided in ESM) of 219 % and 950 % when predicted using the $d_{4,3}$ or d_{90} respectively. However, the inertial flow modified *i*-FMRZ model produces closer predictions with M.A.P.E. values of 69.8 % when using the $d_{4,3}$ average floc size (Fig. 7C) and 43.2 % when using the d_{90} value (Fig. 7D). Heath et al. [32] argued that for concentrated suspensions, the hindered settling effects due to the constriction of inter-particulate spacing and flow effects from preceding particles displacing fluid in their axial-sedimentary path are of greater magnitude than shape and drag effects, which could therefore be neglected. However, Vahedi and Gorczyca [39] found for porous lime softening flocs that drag effects were crucial for first order approximation of settling rates of individual flocs. This suggests that there is a nexus point between the *i*-FMRZ model and the FMRZ model where both effects are at play that is demonstrated in this work.

The role of solids concentration, Φ, was further probed in systems without polymer flocculant (so the sludge properties would be maintained across a concentration range). Fig. 8A presents an example image showing a relatively high concentration of the non-settling β-phase. The sensitivity of the *i*-FMRZ model predictions was probed through multivariate analysis (Fig. 8B) to investigate the change in the required fractal dimension to produce parity with experimental results for varying solids concentration. It was found that compared to fractal dimension, the functional permeability had little influence on the final predicted zonal settling velocity over the range of 0.1–1.0 vol%, as shown in Fig. 8C, indicating that the presence of non-settling fines in the β-phase are not significantly impactful on the settling properties. A key caveat to this argument is that the functional permeability, f_s, of the flocs also has a non-linear relationship to fractal dimension, where small changes in fractal dimension can counteract large changes in solids concentration to achieve the same settling characteristics. This means that the segregation of the β-phase from the αβ-phase could provide an increase in the functional permeability resulting in the greater than modelled (*i*-FMRZ, d_{90}; Fig. 7D) experimental results. Future work will include probing the solids concentration transition point from the FMRZ model to the *i*-FMRZ model.

The sensitivity to the model was further probed, to understand the importance of relative changes to fractal dimension and floc size values in the *i*-FMRZ model, by considering the recalculation of model parameters to give parity with experimental settling data [8]. Table 2 shows recalculated size and fractal dimension values, based on
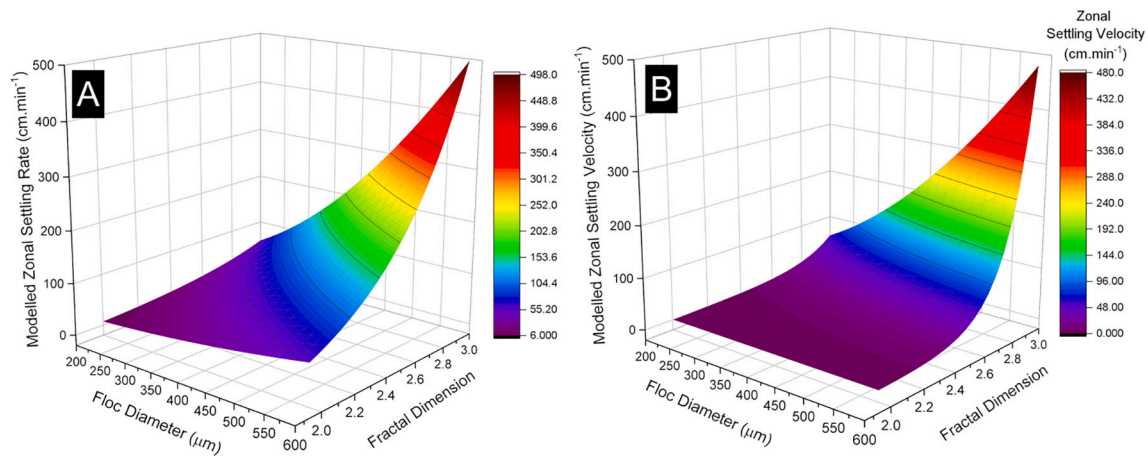
Fig. 6. Multivariate analysis on the impact of fractal dimension and floc diameter on the initial zonal settling rate, $\overline{D_f}$, of 0.84 vol% sludge, using A) a fractal-modified Richardson-Zaki hindered settling model (FMRZ) see Eq. (11) and B) inertial modified *i*-FMRZ model, see Eq. (12). Here, properties of sludge flocculated with 5 ppm FLOPAM are used, as measured by light scattering, where specifically, $\rho_p = 1416.8$ kg·m^{-3} and $D_f/D_p = 10/1.5$.

measured data for settling rates from systems with 0–10 ppm polymer flocculant. The relative differences (%) between the measured and recalculated model floc sizes were much larger to reach parity (46–203 %) when keeping the fractal dimension constant than for the reverse case. Additionally, the calculated sizes required to reach parity across the FLOPAM range did not follow the experimental trend observed in Fig. 5B, with floc size appearing to be independent of polymer dose. The relative differences in measured and recalculated fractal dimensions were much lower to reach parity compared to relative changes in floc size (<6 % or <2.1 % excluding the 0 ppm data point), reinforcing the dominance of fractal dimension in fractal modified hindered settling models. It also highlights that due to this dominance, independent measurements of floc size are very important for validation purposes, at

least when only a single concentration is considered, and thus, caution must be applied when extracting floc sizes from settling rate data.

A final comment is made regarding the consideration of risk and practicality of this research when it comes to deploying technology and models in the nuclear decommissioning sector. Traditionally ex situ methods have been used for characterisation in this context, and therefore sampling from the nuclear facilities in a safe manner, whilst maintaining the scientific integrity is paramount. For example, consider sampling from the fuel storage ponds; where high shear techniques (e.g., centrifugal pumps) have been shown to densify floc structures [8] which could have effects on model predictions. However, this shear would also reduce floc sizes meaning zonal settling projections potentially mitigating the error [65]. When dealing with heterogenous material such as
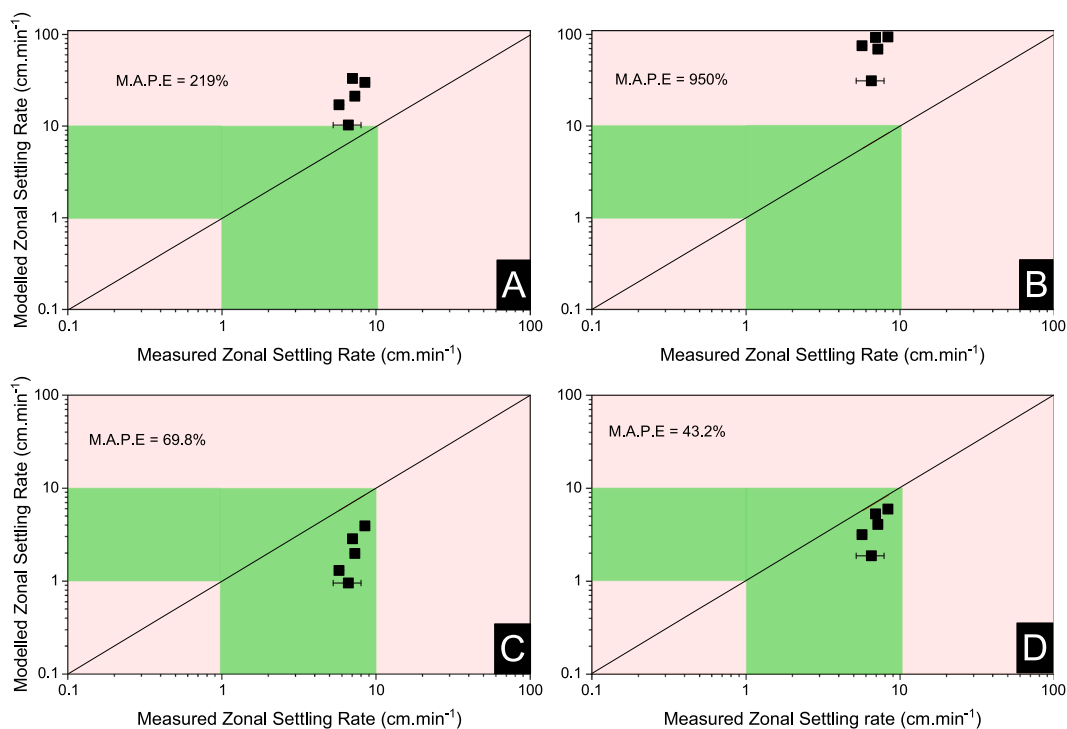
Fig. 7. A parity comparison between experimental data and model prediction of zonal settling rates of sludge flocculated with FLOPAM (0–10 ppm). A and B show the fractal modified Richardson-Zaki (FMRZ) hindered settling model comparison, using the measured volume weighted floc diameter average ($d_{4,3}$) and the 90th cumulative percentile volume weight floc size (d_{90}) respectively. C and D show the inertial flow modified, *i*-FMRZ model using the same sizes respectively. M.A.P.E. is mean absolute percentage error. Green shading represents the order of magnitude of experimental observation.
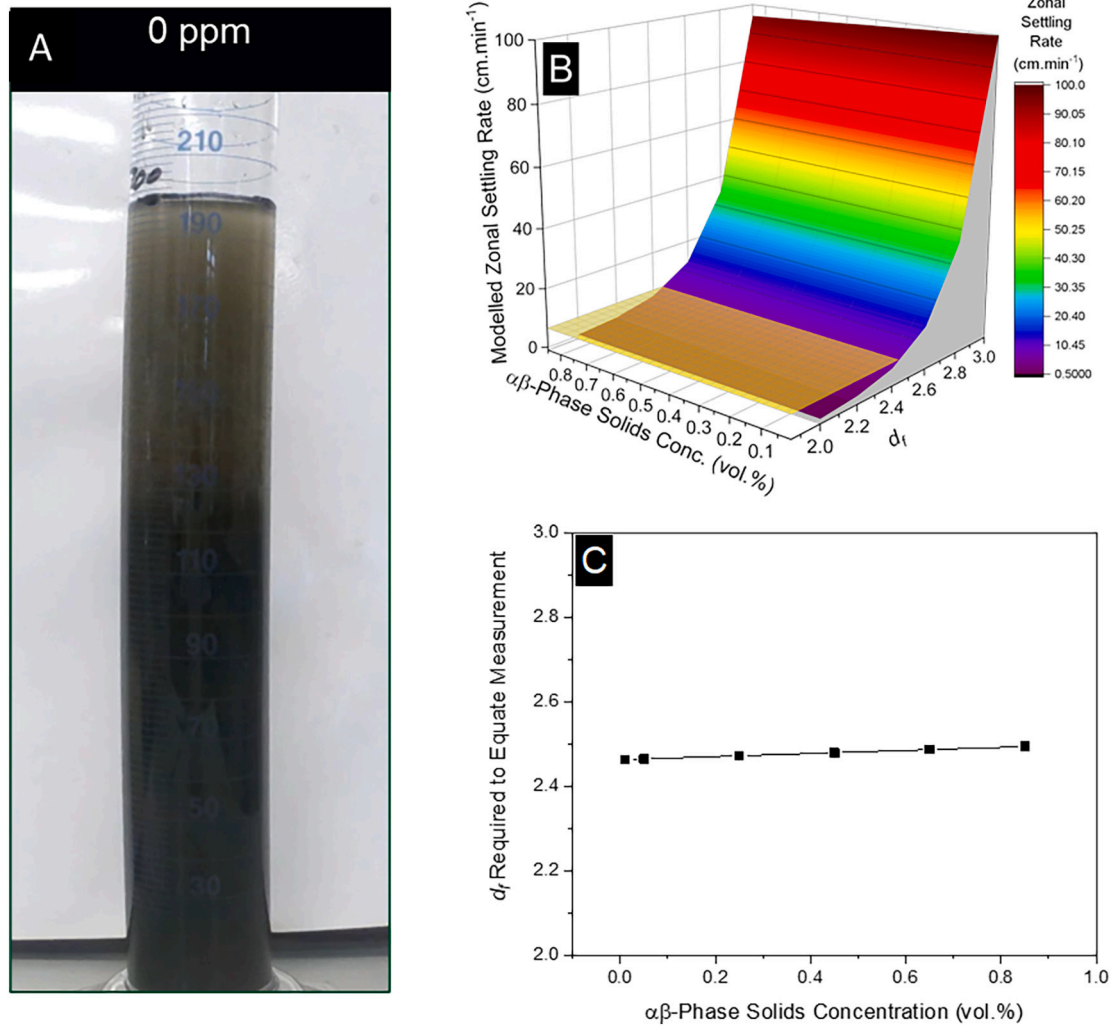
Fig. 8. A) An image of a 0.84 vol% sludge without the presence of FLOPAM FA 920 SEP, showing a significantly turbid supernatant after 8 min of settling. B) A multivariate analysis of the inertial flow modified *i*-FMRZ model, using parameters $\rho_p = 1416.8$ kg·m^{-3} $D_f/D_p = 6.3/1.5$ and $\overline{D_f}$ 256 μm. The intercepting surface indicates the change in fractal dimension required to equate to the observed settling velocity with changing αβ-phase solids concentrations. C) Required fractal dimension to equate the measured zonal settling rate with changes in solids concentration (results of the intercepting plane in B).

Table 2

Investigation of model bias to changes in fractal dimension and floc diameter from the inertial flow modified *i*-FMRZ model (Eq. (12)) to reach parity with observed experimental zonal settling data of sludge dosed with 0–10 ppm of FLOPAM. The top data isolates the independently measured fractal dimension and varies the value of the floc diameter to reach experimental parity with the measure zonal settling rates. The bottom set of data isolates the measured floc diameter and varies the fractal dimension to reach parity.

Polymer conc. (ppm)	0	1.25	2.5	5	10
Recalculated floc size, $\overline{D_f}$, using the *i*-FMRZ model from measured U_i with measured d_f					
Recalculated $\overline{D_f}$ (μm)	778	750	711	683	841
Relative difference (%)	203	70	67	29	46
Estimating fractal dimension using the *i*-FMRZ model from measured U_i with measured $\overline{D_f}$					
Recalculated d_f	2.49	2.36	2.40	2.35	2.35
Relative difference (%)	11.1	4.6	4.6	2.2	2.9
Recalculated ρ_f (kg·m^{-3})	1169	1111	1113	1091	1083
Relative difference (%)	5.7	1.9	2.1	0.8	1.2

the organic/inorganic amalgamations found in open air nuclear storage ponds, one must consider the reliability of physical properties such as refractive index when using structural characterisation techniques that utilise Mie theory. The structural characteristics are dependent on the wave scatter vector, Q, and the scatter intensity which is in itself a function of Q (Eq. (1)), specifically the scatter angle θ. As Q is directly proportional to the refractive index, n, thus small changes would result in changes to Q and $I(Q)$ and the fractal dimension d_f. However, the minimum repeating floc size, D_f, and primary particle sizes, D_p, would also change reducing the magnitude of impact on the fractal modifications to zonal settling models, which is practical serendipity for nuclear waste characterisation that is infamously heterogeneous.

It should be noted that in situ techniques for measuring particle size distributions and properties such as the fractal dimension are being developed such as acoustic backscatter, which have previously been used in tandem with the FMRZ model by Hunter et al. [25], giving confidence to the technology and technical readiness level of this approach in industry. Overall, whilst there is some deviation from parity, the modified *i*-FMRZ model provides a close first order approximation of the zonal settling rate in these complex hindered settling, fractal

systems, providing a basis for residence time prediction in settling stages, improving clarification of operational liquors and reducing risk to the environment.

4. Conclusions

A composite sludge with high organic content was characterised to determine physical and surface chemistry properties and used as a non-radioactive surrogate test material for nuclear waste solid-liquid separation operations. The absolute density value of the sludge was found to be between clays and anaerobic sludges in water facilities, indicating a composite of organic and inorganic material. Pennate and centric diatoms were identified using scanning electron microscopy which are known for having cells stabilised with dominant anionic surface speciation that was confirmed using electrophoresis. Non-ionic FLOPAM polyacrylamide effectively flocculated the sludge material, significantly improving zonal settling rates and supernatant turbidity by an order of magnitude. Whilst the absolute adsorption of the polymer could not be explicitly quantified due to the background of organic material in the sludge, supernatant turbidity and TOC data indicated high adsorption affinity, reducing downstream processing burdens for the local sludge treatment plant, restricting the burden to downstream processes. Over a large polymer dose range, the zonal settling velocity and supernatant turbidity displayed an inflection point indicating an optimum performance and steric stabilisation phenomenon. Furthermore, dosages five times the optimum resulted in only minor decreases in performance with no indication of colloidal stabilisation.

Importantly, a fractal modified Richardson-Zaki power-law hindered settling model was further modified to take account of internal flow and drag effects (called here the 'i-FRMZ' model) and compared to experimental size and settling data. It was found to produce significantly lower error when validated with experimental results, especially when using the measured 90th percentile cumulative size of the flocs, rather than the mean. The model was also found to be particularly sensitive to fractal dimension via multivariate analysis. Further work to identify the nexus point between hindered settling dominance and inertia flow drag dominance has been proposed.

Nomenclature

d_f	Fractal dimension, –
$\overline{D_f}$	Measured diameter of floc, μm
D_f	Diameter of minimum repeating floc unit, μm
D_p	Diameter of primary particles, μm
f_s	Functional permeability of suspension, –
g	Gravitational acceleration, m·s^{-2}
$I(Q)$	Scatter intensity, –
n	Refractive index, –
N	Number of primary particles in a floc, –
Q	Scatter wave vector, μm^{-1}
Re	Particle-floc Reynolds number, –
r_i	Fractal radii, μm
R_z	Richardson-Zaki exponent, –
U_T	Terminal settling velocity, cm·min^{-1}
U_z	Zonal settling velocity, cm·min^{-1}
V_f	Volume of a minimum repeating floc unit, m^3
V_p	Volume of primary particles, m^3
θ	Scatter angle, °
λ	Wavelength, μm
μ_w	Dynamic viscosity of water, kg·m^{-1}·s^{-1}
ρ_f	Density of floc, kg·m^{-3}
ρ_p	Density of primary particle, kg·m^{-3}
ρ_w	Density of water, kg·m^{-3}
Φ	Solids concentration, vol%
ψ	Structure prefactor, –

CRediT authorship contribution statement

Alexander P.G. Lockwood: Conceptualization, Investigation, Methodology, Data curation, Formal analysis, Writing – original draft. **Jacob R.L. Rumney:** Investigation, Data curation, Formal analysis, Writing – review & editing. **Martyn G. Barnes:** Project administration, Writing – review & editing. **Jonathan M. Dodds:** Project administration, Formal analysis, Writing – review & editing. **Jeffrey Peakall:** Formal analysis, Validation, Writing – review & editing. **Timothy N. Hunter:** Conceptualization, Methodology, Investigation, Validation, Funding acquisition, Writing – review & editing.

Declaration of competing interest

The authors declare that they have no known competing financial interests or personal relationships that could have appeared to influence the work reported in this paper.

Data availability

Data will be made available on request.

Environmental implication

The ability to improve sludge thickening efficacy potentially accelerates the decommissioning of nuclear waste management facilities dealing with organic/inorganic composite nuclear waste suspensions. This reduces the risk of environmental release of hazardous materials, as well as likely reducing the economic burden on the taxpayer regarding the volumetric requirements of a geological disposal facility.

Appendix A. Supplementary data

Supplementary data to this article can be found online at https://doi.org/10.1016/j.jwpe.2022.103459.

References

[1] L. Arnold, Windscale 1957: Anatomy of a Nuclear Accident, Palgrave Macmillan, 2007.
[2] S.D. Woodall, M. Hambley, J. Rawcliffe, D. Wiley, D. Hambley, Characterisation of corrosion products from degraded uranium dioxide fuel, J. Nucl. Mater. 552 (2021), 152986.
[3] J.J. Hastings, D. Rhodes, A.S. Fellerman, D. Mckendrick, C. Dixon, New approaches for sludge management in the nuclear industry, Powder Technol. 174 (1–2) (2007) 18–24.
[4] S.F. Jackson, S.D. Monk, Z. Riaz, An investigation towards real time dose rate monitoring, and fuel rod detection in a first generation magnox storage pond (FGMSP), Appl. Radiat. Isot. 94 (2014) 254–259.
[5] J.A. Hope, J. Malarkey, J.H. Baas, J. Peakall, D.R. Parsons, A.J. Manning, S.J. Bass, I.D. Lichtman, P.D. Thorne, L. Ye, D.M. Paterson, Interactions between sediment microbial ecology and physical dynamics drive heterogeneity in contextually similar depositional systems, Limnol. Oceanogr. 65 (2020) 2403–2419.
[6] D.R. Parsons, R.J. Schindler, J.A. Hope, J. Malarkey, J.H. Baas, J. Peakall, A. J. Manning, L. Ye, S. Simmons, D.M. Paterson, R.J. Aspden, S.J. Bass, A.G. Davies, I. D. Lichtman, P.D. Thorne, The role of biophysical cohesion on subaqueous bed form size, Geophys. Res. Lett. 43 (2016) 1566–1573.

[7] F. AlMubaddal, K. AlRumaihi, A. Ajbar, Performance optimization of coagulation/flocculation in the treatment of wastewater from polyvinyl chloride plant, J. Hazard. Mater. 161 (1) (2009) 431–438.

[8] A.P.G. Lockwood, J. Peakall, N.J. Warren, G. Randall, M. Barnes, D. Harbottle, T. N. Hunter, Structure and sedimentation characterisation of sheared Mg(OH)$_2$ suspensions flocculated with anionic polymers, Chem. Eng. Sci. 231 (2021), 116274.

[9] E.A. Lopez-Maldanado, M.T. Oropeza-Guzman, J.L. Juado-Baizaval, A. Ochoa-Teran, Coagulation-flocculation mechanisms in wastewater treatment plants through zeta potential measurement, J. Hazard. Mater. 279 (2014) 1–10.

[10] S. Verma, B. Prasad, I.M. Mishra, Pretreatment of petrochemical wastewater by coagulation and flocculation and the sludge characteristics, J. Hazard. Mater. 178 (1–3) (2010) 1055–1064.

[11] W.R. Bower, K. Morris, J.F.W. Mosselmans, O.R. Thompson, A.W. Banford, K. Law, R.A.D. Pattrick, Characterising legacy spent nuclear fuel pond materials using microfocus X-ray adsorption spectroscopy, J. Hazard. Mater. 317 (2016) 97–107.

[12] J.M. Henderson, A.D. Wheatley, Factors effecting a loss of flocculation activity of polyacrylamide solutions: shear degradation, cation complexation, and solution aging, J. Appl. Polym. Sci. 33 (2) (1987) 669–684.

[13] Z. Maher, P. Ivanov, L. O'Brien, H. Sims, R.J. Taylor, S.L. Heath, F.R. Livens, D. Goddard, S. Kellet, P. Rand, N.D. Bryan, Americium and plutonium association with magnesium hydroxide colloids in alkaline nuclear industry process environments, Journal of Nuclear Materials. 468 (2015) 84–96.

[14] J. Gregory, S. Barany, Adsorption and flocculation by polymers and polymer mixtures, Adv. Colloid Interface Sci. 169 (1) (2011) 1–12.

[15] Y. Ji, Q. Lu, Q. Liu, H. Zeng, Effect of solution salinity on settling of mineral tailings by polymer flocculants, Colloids Surf. A Physiochem. Eng. Asp. 420 (2013) 29–38.

[16] F. Roselet, D. Vandamme, M. Roselet, K. Muylaert, P.C. Abreu, Screening of commercial natural and synthetic cationic polymers for flocculation of freshwater and marine microalgae and effects of molecular weight and charge density, Algal Res. 10 (2015) 183–188.

[17] T. Swift, L. Swanson, A. Bretherick, S. Rimmer, Measuring poly(acrylamide) flocculants in fresh water using inter-polymer complex formation, Environ. Sci. Water Res. Technol. 1 (2015) 332–340.

[18] A. Pugazhendhi, S. Shobana, P. Bakonyi, N. Nemestothy, A.Rajesh Xia, J. Banu, G. Kumar, A review on chemical mechanism of microalgae flocculation via polymers, Biotechnol Rep. (Amst) 21 (2019), e0032.

[19] A. Sukenik, D. Bilanovic, G. Shelef, Flocculation of microalgae in brackish and sea waters, Biomass 15 (3) (1988) 187–199.

[20] L.F. Mortimer, M. Fairweather, Prediction of polymer extension, drag reduction, and vortex interaction in direct numerical simulation of turbulent channel flows, Phys. Fluids 34 (2022), 073318.

[21] H. Lee, S. Chang, T. Kim, S. Park, H. Jeon, Effective treatment of uranium-contaminated soil-washing effluent using precipitation/flocculation process for water reuse and solid waste disposal, J. Water Proc. Engr. 48 (2022), 102890.

[22] G. Atesok, P. Somasundaran, L.J. Morgan, Charge effects in the adsorption of polyacrylamide on sodium kaolinite and its flocculation, Powder Technol. 54 (2) (1988) 77–83.

[23] G.P. Karmakar, K.K. Chandan, Flocculation behaviour of bentonite clay-water systems, Adv. Mater. Process. Technol. 5 (1) (2019) 1–14.

[24] A.I. Nakatani, C.E. Mohler, S. Hughes, Chain conformation of polymers adsorbed to clay particles: effects of charge and concentration, Soft Matter 17 (2021) 6848–6862.

[25] T.N. Hunter, J. Peakall, D. Egarr, D.M.J. Cowell, S. Freear, A.S. Tonge, L. Horton, H.P. Rice, I. Smith, K. Malone, D. Burt, M. Barnes, G. Randall, S. Biggs, M. Fairweather, Concentration profiling of a horizontal sedimentation tank utilising a bespoke acoustic backscatter array and CFD simulations, Chem. Eng. Sci. 218 (2020), 115560.

[26] S.T. Hussain, J. Peakall, M.G. Barnes, T.N. Hunter, Characterizing Flocculated Suspensions with an Ultrasonic Velocity Profiler in Backscatter Mode, IEEE International Ultrasonics Symposium (IUS), Xi'an, China, 2021.

[27] T. Gonzalez, J.R. Dominguez, J. Beltran-Heredia, H.M. Garcia, F. Sanchez-Lavado, Aluminium sulfate as coagulant for highly polluted cork processing wastewater: evaluation of settleability parameter and design of clarifier thickening uni, J. Hazard. Mater. 148 (1–2) (2007) 6–14.

[28] Y. Kim, W.O. Pipes, Factors influencing suspended solids concentrations in activated sludge settling tanks, J. Hazard. Mater. 67 (1) (1999) 95–109.

[29] A.P.G. Lockwood, N.J. Warren, J. Peakall, S. Hussain, G. Randall, M.G. Barnes, D. Harbottle, T.N. Hunter, A comparison of the sedimentation dynamics of statistical and deblock copolymer flocculation aids in radwaste dewatering, in: Waste Management Symposium, 2021. Phoenix, Arizona USA.

[30] J.F. Richardson, W.N. Zaki, The sedimentation of a suspension of uniform spheres under conditions of viscous flow, Chem. Eng. Sci. 8 (1954) 65–73.

[31] S.M. Glover, Y. Yan, G.J. Jameson, S. Biggs, Bridging flocculation studied by light scattering and settling, Chem. Eng. J. 80 (1–3) (2000) 3–12.

[32] A.R. Heath, P.A. Bahri, P.D. Fawell, J.B. Farrow, Polymer flocculation of calcite: relating aggregate size to settling rate, AIChEJ. 52 (6) (2006) 1987–1994.

[33] M. Rhodes, Introduction to Particle Technology, Wiley, 2008.

[34] G.C. Bushell, Y.D. Yan, D. Woodfield, J. Raper, R. Amal, On techniques for the measurement of the mass fractal dimension of aggregates, Adv. Colloid Interface Sci. 95 (2002) 1–50.

[35] C.P. Johnson, X. Li, B.E. Logan, Settling velocities of fractal aggregates, Environ. Sci. Technol. 30 (1996) 1911–1918.

[36] F. Maggi, The settling velocity of mineral, biomineral, and biological particles and aggregates in water, J. Geophys. Res: Oceans. 118 (2013) 2118–2132.

[37] I.A. Mola, P.D. Fawell, M. Small, Particle-resolved direct numerical simulation of drag force on permeable, non-spherical aggregates, Chem. Eng. Sci. 8 (2020), 115582.

[38] A. Vahedi, B. Gorczyca, Predicting the settling velocity of flocs formed in water treatment using multiple fractal dimensions, Water Res. 46 (13) (2012) 4188–4194.

[39] A. Vahedi, B. Gorczyca, Settling velocities of multifractal flocs formed in chemical coagulation process, Water Res. 53 (2014) 322–328.

[40] Z. Zhu, A formula for the settling velocity of cohesive sediment flocs in water, Water Supply 19 (5) (2019) 1422–1428.

[41] A.P.G. Lockwood, P. Kok Shun, J. Peakall, N.J. Warren, T. Barber, N. Basharat, G. Randall, M.G. Barnes, D. Harbottle, T.N. Hunter, Flotation using sodium dodecyl sulphate and sodium lauryl isethionate for rapid dewatering of Mg(OH)$_2$ suspensions, RSCAdvances 11 (2021) 18661.

[42] E. Asensi, E. Alemany, A hindered settling velocity model related to the fractal dimension and activated sludge flocs characteristics: application to a sludge with a previous fragmentation and flocculation process, Sep. Purif. Technol. 300 (2022), 121812.

[43] M.J. Johnson, J. Peakall, M. Fairweather, S. Biggs, D. Harbottle, T.N. Hunter, Characterisation of multiple hindered settling regimes in aggregated mineral suspensions, I&EC Res. 55 (2016) 9983–9993.

[44] C. Kang, Y. Zhao, C. Tang, O. Addo-Bankas, Use of aluminium-based water treatment sludge as coagulant for animal farm wastewater treatment, J. Water Proc. Engr. 46 (2022), 102645.

[45] B.B. Mandelbrot, Fractals: Form, Chance and Dimension, W. H. Freeman, 1977.

[46] C.M. Sorensen, Light scattering by fractal aggregates: a review, Aerosol Sci. Technol. Am. Assoc. Aerosol Res. 35 (2001) 648–687.

[47] G.V. Franks, Y. Zhou, Y. Yan, G.J. Jameson, S. Biggs, Effect of aggregate size on sediment bed rheological properties, Phys. Chem. Chem. Phys. 6 (2004) 4490–4498.

[48] L. Gmachowski, Mechanism of shear aggregation, Water Res. 29 (1995) 1815–1820.

[49] M.S. Nasser, A.E. James, The effect of polyacrylamide charge density and molecular weight on the flocculation and sedimentation behaviour of kaolinite suspensions, Sep. Purif. Technol. 52 (2) (2006) 241–252.

[50] M. Qasim, S. Park, J. Kim, Empirical Reynolds number model for drag coefficient determination of ballasted flocs, J. Water Proc. Engr. 40 (2021), 101803.

[51] J.C. Winterwerp, A simple model for turbulence induced flocculation of cohesive sediment, J. Hydraul. Res. 36 (1998) 309–326.

[52] L. Schiller, A. Naumann, A drag coefficient correlation, Zeitschrift des Vereins Deutscher Ingenieure. 77 (1933) 318–320.

[53] F. Xiao, K.M. Lam, X. Li, Investigation and visualization of internal flow through particle aggregates and microbial flocs using particle image velocimetry, J. Colloid Interface Sci. 397 (2013) 163–168.

[54] L. Caizán-Juanarena, A. Heijne, J. Weijma, D. Yntema, D.A. Suárez-Zuluaga, C.J. N. Buisman, Screening for electrical conductivity in anaerobic granular sludge from full-scale wastewater treatment reactors, Biochem. Eng. J. 159 (2020), 107575.

[55] L. van den Berg, M. van Pronk, M.C.M. de Loosdrecht, M.K. Kreuk, Density measurements of aerobic granular sludge, Environ. Technol. (2022), https://doi.org/10.1080/09593330.2021.2017492.

[56] A. Kumar, B.K. Hodnett, S. Hudson, P. Davern, Modification of the zeta potential of montmorillonite to achieve high active pharmaceutical ingredient nanoparticle loading and stabilization with optimum dissolution properties, Colloids Surf. B: Biointerfaces 193 (2020), 111120.

[57] D. Bilanovic, G. Shelef, A. Sukenik, Flocculation of microalgae with cationic polymers-effects of medium salinity, Biomass 17 (1) (1988) 65–76.

[58] S.A. Walling, M.N. Kauffmann, L.J. Gardner, D.B. Bailey, M.C. Stennett, C. L. Corkhill, N.C. Hyatt, Characterisation and disposability assessment of multi-waste stream in-container vitrified products for higher activity radioactive waste, J. Hazard. Mater. 401 (2021), 123764.

[59] A. Vahedi, B. Gorczyca, Application of fractal dimensions to study the structure of flocs formed in lime softening process, Water Res. 45 (2) (2011) 545–556.

[60] R.K. Chakraborti, K.H. Gardner, J.F. Van Atkinson, J.E. Benschoten, Changes in fractal dimension during aggregation, Water Res. 37 (4) (2003) 873–883.

[61] P. Jarvis, S.A. Parsons, R. Henderson, N. Nixson, B. Jefferson, The practical application of fractal dimension in water treatment Practice–the impact of polymer dosing, Sep. Sci. Technol. 43 (7) (2008) 1785–1797.

[62] M.S. Nasser, Characterisation of floc size and effective floc density of industrial papermaking suspensions, Sep. Purif. Technol. 122 (2014) 495–505.

[63] Y.Q. Zhao, Correlations between floc physical properties and optimum polymer dosage in alum sludge conditioning and dewatering, Chem. Eng. J. 91 (1–3) (2003) 227–235.

[64] J. Garside, M.R. Al-Dibouni, Velocity-voidage relationships for fluidisation and sedimentation in solid-liquid phases, Ind. Eng. Chem. Proc. Des. Dev. 16 (1977) 206.

[65] G.V. Franks, P.D. Yates, N.W.A. Lambert, G.J. Jameson, Aggregate size and density after shearing, implications for dewatering fine tailings with hydrocyclones, Int. J. Miner. Process. 77 (1) (2005) 46–52.

[66] N. Paul, S. Biggs, J. Shiels, R.B. Hammond, M. Edmondson, L. Maxwell, D. Harbottle, T.N. Hunter, Influence of shape and surface charge on the sedimentation of spheroidal, cubic and rectangular cuboid particles, Powder Technol. 322 (2017) 75–83.